Analysis of Modern Optimal Control Theory Applied to Plasma Position and Current Control in TFTR

M.A. Firestone

Princeton University Plasma Physics Laboratory

Princeton, New Jersey 08544

Abstract

The strong compression TFTR discharge has been segmented into regions where linear dynamics can approximate the plasma's interaction with the OH and EF power supply systems. The dynamic equations for these regions are utilized within the linear optimal control theory framework to provide active feedback gains to control the plasma position and current. Methods are developed to analyze and quantitatively evaluate the quality of control in a nonlinear, more realistic simulation. Tests are made of optimal control theory's assumptions and requirements, and the feasibility of this method for TFTR is assessed.

Table of Contents

I. Introduction

Plasma position and current control is a matter of significant concern for the next generation of large tokamaks. The use of modern optimal control theory provides the most "scientific" basis for determining a feedback control strategy when dealing with complex coupled phenomena in a multi-input/ multi-output system. In recent years there have been several attempts[1-4] to apply optimal control in a practical sense to large tokamaks. However, an independent analysis of optimal control in tokamaks has not yet emerged. Only previous work by this author[2] has provided an independent verification of optimal control feedback gains. The objective of this paper will go beyond verification; it will attempt to provide an analysis and evaluation of the robustness of the optimal control approach.

The procedure of gain determination in optimal control theory requires minimization of a performance integral, much as in calculus of variations. However, there are several variables to be minimized and there is no straightforward method for weighting them in the performance integral. Thus, we have the uncomfortable situation in which a multitude of "optimal" gain sets can be determined, some of them quite bizarre! This makes a black box approach to optimal gain determination impossible and discourages its use. By taking cognizance of the differences between the simplified linear dynamics, which is the domain of linear optimal control theory, and the actual experimental situation, with its inherent complexities, much of the confusion can be eliminated. These differences are explored quantitatively by utilizing a modified version of the Plasma-Circuit Interaction Code[5] and comparing these results with those predicted from the linear theory.

An inherent simplification has been made in this work by neglecting the eddy current and power supply dynamics. Although eddy currents were

considered in previous work,[4,5] a realistic eddy current model simple enough to incorporate into the optimal control code has not yet been developed. Since important time constant modes in the range of 1-10 ms were not included in our earlier filament model, it has been decided not to use that model for this analysis. Another reason to ignore eddy currents at this stage is that they will require measurements in addition to those which directly describe the discharge (i.e., $R, \dot{R}, I_p, \dot{I}_p$). This will in turn make the analysis of the control more complex and ambiguous. Since this first attempt is designed to answer some rather basic questions about optimal control, only the most important poloidal circuits (OH, EF, and plasma) have been incorporated into the model. However, throughout the course of this report, short discussions of eddy current effects will appear. Similarly, simplified power supply dynamics could be incorporated into the model, but this will wait until a realistic power supply simulation is attached to the Plasma-Circuit Interaction Code so that a proper evaluation can be performed.

II. Optimal Control Theory

Since this work is an analysis of optimal control applied to the tokamak problem, only a brief introduction to optimal control theory will be presented here. For details a standard reference[6] can be consulted.

To be amenable to solution by optimal control theory the system dynamics must be represented by:

$$\dot{\underline{X}} = A\,\underline{X} + B\,\underline{u} \qquad \text{(II-1)}$$

$$\underline{Y} = C\,\underline{X} + D\,\underline{u} \ , \qquad \text{(II-2,}$$

where $\underline{X}$ is the state vector entirely describing the linear system, $\underline{u}$ is the control vector, and $\underline{Y}$ is the set of physical measurements from which the state of the system is deduced. The quantities A, B, C, and D are matrices which in principle may be time dependent, but which in our formulation are constant. The discrete-time versions of Eqs. (II-1) and (II-2) are

$$\underline{X}_{K+1} = \Phi(\Delta t)\underline{X}_K + F(\Delta t)\ \underline{u}_K \qquad \text{(II-3)}$$

$$\underline{Y}_K = C\ \underline{X}_K + D\ \underline{u}_K\ , \qquad \text{(II-4)}$$

where

Δt = the sample time,

$\Phi(\Delta t)$ = the state transition matrix evaluated at Δt (i.e, $e^{A\Delta t}$),

$F(\Delta t) = \int_0^{\Delta t} \Phi(\Delta t - \tau)\ B(\tau)\ d\tau$.

The optimal control $\underline{u}^*$ is obtained by minimizing the performance index

$$J = \int_{t_o}^{T} (\underline{X}^T Q\ \underline{X} + \underline{u}^T R\ \underline{u}) dt \qquad \text{(II-5)}$$

subject to the system dynamics Eq. (II-1). Here Q and R are weighting matrices which determine the emphasis placed in controlling the various state variables, Q, and on minimizing the amount of control, R. The discrete version is obtained from Eq. (II-5) and the fact that the controls are held fixed over the sample interval Δt:

$$J = \sum_{K=1}^{N} \left(\underline{X}_K^T\ \tilde{Q}\ \underline{X}_K + 2\ \underline{u}_K^T\ \tilde{S}\ \underline{X}_K + \underline{u}_K^T\ \tilde{R}\ \underline{u}_K\right)\ , \qquad \text{(II-6)}$$

where

$$\tilde{Q} = \int_{o}^{\Delta t} \Phi^{T}(\Delta t-\tau)\, Q\Phi(\Delta t-\tau)d\tau \ ,$$

$$\tilde{S} = \int_{o}^{\Delta t} F^{T}(\Delta t-\tau)\, Q\Phi(\Delta t-\tau)d\tau \ ,$$

$$\tilde{R} = \int_{o}^{\Delta t} \left[R + F^{T}(\Delta t-\tau)\, QF(\Delta t-\tau)\right]d\tau \ .$$

The optimal control $\underline{u}_K^*$ becomes a linear function of the state variables,

$$\underline{u}_K^* = -\left(\tilde{R} + F^{T}P_{K}F\right)^{-1}\left(F^{T}P_{K}\Phi + \tilde{S}\right)\underline{X}_K \ , \qquad \text{(II-7)}$$

where P_K is the solution of the discrete matrix Riccati equation

$$P_K = \left(\Phi^{T}\, P_{K+1}\Phi + \tilde{Q}\right) - \left(F^{T}P_{K+1}\Phi + \tilde{S}\right)^{T} \qquad \text{(II-8)}$$

$$\cdot \left(\tilde{R} + F^{T}\, P_{K+1}F\right)^{-1}\left(F^{T}\, P_{K+1}\Phi + \tilde{S}\right)$$

with $P_N = [0]$. There are several methods for solving Eq. (II-8) and the procedure used in this work is described in Ref. 7. The continuous problem can be similarly evaluated. It can also be shown[6] that

$$J_{min} = \underline{X}^{T}(t_o)\, P(t_o)\underline{X}(t_o) \qquad \text{(II-9)}$$

which allows the comparison of various control strategies in terms of their overall effectivness.

In practice, the performance index is usually written in terms of the measurements, $\underline{Y}$, since we attempt to minimize the difference between desired and actual response. Hence,

$$J = \int_{t_o}^{T} [(\underline{Y} - \underline{Y}_o)^T Q(\underline{Y} - \underline{Y}_o) + (\underline{u} - \underline{u}_o)^T R (\underline{u} - \underline{u}_o)]dt \qquad \text{(II-10)}$$

where $\underline{Y}_o$ and $\underline{u}_o$ are the desired measurement values and the nominal control to achieve them. The feedback is required to overcome modeling errors and perturbations. Specified in this way Eq. (II-10), or its discrete-time counterpart, can be used to numerically evaluate J from experiment or a realistic computer simulation and the results compared with J_{min} from Eq. (II-9). If there is close agreement, the linear dynamics of Eq. (II-1) can be assumed to be a valid representation of the actual system.

The measurement set $\underline{Y}$ should be chosen according to two criteria. First, $\underline{Y}$ must be a good basis set within which the state variables $\underline{X}$ can be accurately described. If this condition is not met, very ill conditioned matrices will appear in the optimal gain algorithms and the results will be meaningless. Secondly, $\underline{Y}$ should as much as possible directly describe the discharge and the variables to be controlled. Thus, plasma current and major radius are "direct" variables whereas power supply currents are "indirect" for our purposes.

Finally, we should consider the costs and benefits of optimal control theory. The main benefits are two. First, as previously mentioned, it is the only way to specify the best overall control for a coupled multi-variable system. We obtain the optimal feeback control gains given a set of priorities (the performance index weights). Secondly, optimal control with full state feedback has infinite gain margin and is absolutely stable about the point at

which the linear model was derived. It also has at least 60 degrees of phase margin. Therefore, the optimal design will be relatively insensitive to modeling errors and noise. The costs are that we must produce linear models and use full state feedback (one feedback for every state variable). We will examine these assumptions in the following sections.

III. Linear Control Dynamics

The linear model is comprised of the circuit equations and the Shafranov equilibrium equation.[8] The vertical field required to maintain horizontal stability is

$$B_v = \frac{\mu_o I_p}{4\pi R}\left[\ell n\left(\frac{8R}{a}\right) - \frac{3}{2} + \frac{\ell_i}{2} + \beta_\theta\right] , \qquad \text{(III-1)}$$

where: $\beta_\theta = \gamma\beta_\theta^*$,

R = plasma major radius,

I_p = plasma current,

a = plasma minor radius,

$\ell_i/2$ = plasma internal inductance,

β_θ^* = ratio of plasma pressure to poloidal magnetic field pressure,

γ = 1. for isotropic pressure, otherwise depends upon orientation of neutral beam ions.

In addition the quantities vary according to:

i) $a \propto \sqrt{R}$ after plasma has grown to final size.

ii) $a + R = a_o + R_o$, plasma growth model during startup.

iii) $\ell_i/2 \propto R^{-2} I_p^{-2}$ after plasma growth.

iv) $\beta_\theta \propto R^{-7/3} I_p^{-2}$.

Assumption i) comes from toroidal flux conservation and the fact that $B_T \propto R^{-1}$; iii) from assuming q is approximately constant over the plasma; iv) assumes density and temperature profiles of $n \propto R^{-2}$ and $T \propto R^{-4/3}$.

The β_θ time history has been modeled as

$$\beta_\theta = Ke^{-\omega t} [\sin\omega t + \cos\omega t] \quad , \qquad \text{(III-2)}$$

where K and ω are chosen to match $\dot{\beta}_\theta(0)$ and the maximum β_θ from the Plasma-Circuit Interaction Code simulations. Although the time to reach the maximum is incorrect, the important criterion is providing a realistic $\dot{\beta}_\theta(0)$. The control is relatively insensitive to the exact β_θ as will be seen in Section V.

The circuit equations are

$$\frac{d}{dt}(L\underline{I}) + \hat{R}\,\underline{I} = \underline{V} \qquad \text{(III-3)}$$

where:

L is the matrix of self and mutual inductances between the plasma, EF, OH, (eddy currents).

$\underline{I}$ is a vector containing the individual currents, (I_{OH}, I_{EF}, I_p, $\{I_{eddy}\}$).

$\hat{R}$ is the matrix of circuit resistances.

$\underline{V}$ is the power supply voltage vector (OH and EF).

Since all of the inductance terms that relate to the plasma are functions of R, the circuit equations are nonlinear. In order to utilize optimal control theory we must linearize our state variable equation about some nominal operating point. The procedure is as follows:

$$\frac{d}{dt}(L\underline{I}) = \frac{dL}{dR}\,\underline{I}\,\frac{dR}{dt} + L\,\frac{d\underline{I}}{dt}\,, \tag{III-4}$$

where dR/dt is obtained by differentiating the Shafranov Eq. (III-1) to obtain

$$\frac{dR}{dt} = \underline{w}^T\,(R,\ I_p,\ I_{EF},\ \{I_K\})\,\frac{d\underline{I}}{dt} + \left(\frac{\partial R}{\partial \beta_\theta}\right)\frac{\partial \beta_\theta}{\partial t}\,, \tag{III-5}$$

($\{I_K\}$ are eddy currents). Here the vertical field has been expressed in terms of I_{EF} and $\{I_K\}$.[1]

The linearization proceeds by choosing nomimal operating currents $\underline{I}_o$, which then imply a nominal R_o and L_o matrix. Then the currents, major radius, and inductance matrix are represented in terms of the nominal and perturbed values as:

$$\begin{aligned} \underline{I} &= \underline{I}_o + \varepsilon\underline{I}_1, \\ R &= R_o + \varepsilon R_1, \\ L &= L_o + \varepsilon L_1. \end{aligned} \tag{III-6}$$

We now consider the time derivative of the first order perturbed flux:

$$\frac{d}{dt}(LI)_1 = L_o \frac{d\underline{I}_1}{dt} + L_1 \frac{d\underline{I}_o}{dt} + \underline{I}_o \frac{dL_1}{dt} + \underline{I}_1 \frac{dL_o}{dt}, \qquad \text{(III-7)}$$

where

$$\frac{dL_1}{dt} = \frac{dL_o}{dR}\frac{dR_1}{dt} + \frac{d^2L_o}{dR^2}\frac{dR}{dt} R_1,$$

$$R_1 = \underline{w}^T \underline{I}_1 + \left(\frac{\partial R}{\partial \beta_\theta}\right) \beta_\theta .$$

Thus, the linear differential equation for perturbations away from $\underline{I}_o$ is

$$\left[L_o + \left(\frac{dL}{dR}\right)_o \underline{I}_o \underline{w}_o^T\right] \frac{d\underline{I}}{dt} + \left\{\frac{dR_o}{dt}\left[\left(\frac{dL}{dR}\right)_o + \left(\frac{d^2L}{dR^2}\right)_o \underline{I}_o \underline{w}_o^T\right.\right.$$

$$+ \left(\frac{dL}{dR}\right)_o \underline{I}_o \left(\frac{\partial \underline{w}^T}{\partial R}\right)_o\Big] + \left(\frac{dL}{dR}\right)_o \underline{I}_o \frac{d\underline{I}_o^T}{dt}\left(\frac{\partial \underline{w}}{\partial \underline{I}}\right)_o$$

$$\left. + \left(\frac{dL}{dR}\right)_o \frac{d\underline{I}_o}{dt} \underline{w}_o^T\right\} \underline{I} + \hat{R}\,\underline{I} = \underline{V}_1 + \left(\frac{\partial R}{\partial \beta_\theta}\right)_o \left[\left(\frac{dL}{dR}\right)_o \frac{\underline{I}_o}{dt}\right.$$

$$\left. + \frac{dR_o}{dt}\frac{d^2L_o}{dR^2}\underline{I}_o\right] \beta_\theta + \left[\left(\frac{\partial R}{\partial \beta_\theta}\right)_o \left(\frac{dL}{dR}\right)_o \underline{I}_o\right] \frac{\partial \beta_\theta}{\partial t} \qquad \text{(III-8)}$$

where $\underline{I}_1$ and R_1 have now been renamed $\underline{I}$ and R. This equation shows the importance of large $d\underline{I}_o/dt$ and dR_o/dt which occur during certain phases of the discharge. Note that any of the circuit currents may contribute in this fashion. Equation (III-8) is the linear system dynamics equation corresponding to Eq. (VI-1), with the perturbed currents $\underline{I}$ becoming the state variables $\underline{X}$, totally describing the plasma-poloidal field system. In this framework R corresponds to a measurement.

The linear dynamics of Eq. (III-8) will be valid only in a small region of the discharge centered on the nominal operating point, $\underline{I}_o$. Since the discharge is very nonlinear, it has been broken down into several phases which will then correspond to separate control problems. Each phase has its own operating point, and the terms $\underline{i}_o$, dI_o/dt, $\underline{w}_o$, dR_o/dt, etc., in Eq. III-8) will be specific to the phase. Figure 1 shows the plasma current, major radius, temperature, and β_θ time histories for the strong compression discharge obtained from a "perfect" feedback simulation with the Plasma-Circuit Interaction Code.[5] The discharge is broken up into:

1. Startup -- plasma growth model.
2. Pre-compression -- constant I_p and R, neutral beam heating.
3. Compression -- no control, OH set to "perfect" feedback value to maintain I_p profile.
4. Post-Compression -- final constant I_p, R.
5. Termination -- constant R as I_p is quickly decreased.

Each phase will be modeled separately and its active feedback characteristics analyzed in the sections that follow.

The linear models and resultant computer code were developed in collaboration with R. Gran and M. Rossi of Grumman Aerospace Corp.[1,2] The general optimization codes used in this work were developed by the Grumman Research Department.[7]

IV. Plasma-Circuit Interaction Code (PCIC)

The linear model is used only to determine the system feedback gains. The actual closed loop control is evaluated and analyzed by utilizing the

Plasma-Circuit Interaction Code, PCIC, in its feedback mode. The physics and engineering models incorporated into the code are fully described in Ref. 5. The additions to the code necessitated by the feedback analysis are presented in Appendix A of this report.

The code models the plasma evolution during the various stages of a specified discharge. It contains the nonlinear coupling between the plasma and external poloidal field circuits assuming instantaneous equilibration with the equilibrium vertical field. A plasma growth model is assumed during startup and toroidal flux conservation after the plasma is fully expanded. A one-dimensional current penetration model produces current profiles and values of $\ell_i/2$, the plasma internal inductance required by the Shafranov equation. Particle and energy transport are simulated by a zero dimensional particle and energy balance model where impurities affect the plasma temperature through their radiative energy loss. These are accounted for by incorporating impurity rate equations into the plasma dynamics. Neutral beam heating is modeled as a series of beam slugs deposited into the plasma, heating as they slow down and become thermalized.

The PCIC may be operated in two modes -- "perfect" feedback or real feedback. The "perfect" feedback mode constrains the plasma to behave as ideally desired and computes the required OH and EF power supply currents and voltages. The real feedback mode uses power supply voltages determined from the active feedback to drive the system of coupled plasma-circuit equations. These voltages are reduced if they exceed the characteristic voltage-current limits. Nominal voltages can be determined from "perfect" feedback simulations or from other estimates.

The linear models used in the optimal control work do not compute temperatures, densities, plasma resistance, or β_θ. Instead, an average plasma

resistance is read in as data for each phase of the discharge, and β_θ is modeled according to Eq. (III-2). The resistance and β_θ parameters are determined from "perfect" feedback results.

V. Control During Pre-Compression and Neutral Beam Heating

The first phase we will consider is that of pre-compression where neutral beam heating poses a major control problem. The analysis techniques developed here will then carry over into the other phases of the discharge.

As mentioned previously there is no standard procedure for choosing the weights, Q and R of Eq. (II-5), in the performance index. Since any number of weighting schemes can be chosen, an almost infinite number of "optimal" gain sets can be determined. The method proposed here ties the performance index weights to the physical control objectives. This is accomplished by normalizing all of the terms in the measurement performance index Eq. (II-10), specifying the maximum error for each measurement and the desired control authority (feedback voltages). Thus, a small allowable error will produce a large weight and vice versa. Furthermore, we can have derivative, proportional, and integral terms in the performance index and the weighting will reflect whether instantaneous or long range control is the objective. Except during startup, only proportional and integral terms will be considered since the derivative measurements may be noisy. Table V-1 lists two extreme sets of weights for given R and I_p errors. The proportional set weights only I_p and R, whereas the integral set weights only $\int I_p dt$ and $\int R dt$. The optimal feedback gains for these two sets are displayed in Table V-2. All gain values in this report are in terms of meters, amps, seconds, and volts. In practice, the performance index would include both proportional and integral terms. The integral terms provide the integral compensation of classical control by

reducing steady state DC error. They are introduced in an augmented state variable vector[6] by the relationships $(\int \dot{R}dt) = R$ and $(\int \dot{I}_p dt) = I_p$. Since R is a measurement it is of course expressed in terms of the state variable vector $\underline{I}$. Similarly, β_θ and $\dot{\beta}_\theta$ can become part of the augmented state variable vector during neutral beam heating. It should also be noted from Table V-2 that proportional weighting produces only proportional gains, whereas integral weights produce both proportional and integral gains. This is because the objective of integral weighting is to reduce the integrated error, a component of which is the absolute error. By limiting the instantaneous error, the integrated error can more easily be kept in bounds. This is a subtle difference from the integral compensation in classical control, which is an independent entity. In optimal control it is coupled into the problem via the augmented state variable vector and its influence is felt throughout the entire system.

The basic measurement set $\underline{Y}$ was chosen to be I_p, $\dot{I}_p$, R because this set satisfies the two criteria specified in the previous section. The set I_p, R, $\dot{R}$ can not be utilized because it does not provide a good basis to describe I_{OH} in the state variable vector. However, with more state variables such as eddy currents $\dot{R}$ could be used. This is also true if the OH circuit were taken out of the model (as in start-up, Section VII).

The discrete gains were evaluated assuming a sample time of 1.38 ms, approximating the limitations of the pulsed power supply. Therefore, the feedback voltages are held constant for 1.38 ms.

Table V-1

Pre-Compression Performance Index Weights

	R	I_p	$\int Rdt$	$\int I_p dt$	V_{OH}	V_{EF}
Maximum Deviation	.01 m	3×10^4 amps	10^{-3}	10^4	3×10^3V	3×10^3V
Proportional Weights	10^4	10^{-9}	0.	0.	10^{-7}	10^{-7}
Integral Weights	0.	0.	10^6	10^{-8}	10^{-7}	10^{-7}

Table V-2

Pre-Compression Discrete Feedback Gains

	Proportional Weights		Integral Weights	
	EF	OH	EF	OH
R	1.64×10^5	-1.87×10^4	4.21×10^4	3.73×10^3
$\dot{I}_p$	3.57×10^{-4}	-7.34×10^{-5}	-2.03×10^{-4}	-3.74×10^{-4}
I_p	1.68×10^{-3}	-8.09×10^{-2}	-8.22×10^{-2}	-4.67×10^{-2}
$\int Rdt$	0.	0.	3.02×10^6	4.70×10^5
$\int I_p dt$	0.	0.	2.39×10^{-3}	-3.31×10^{-1}
β_θ	1.15×10^2	2.74×10^2	1.05×10^2	8.15×10^2
$\dot{\beta}_\theta$	1.39×10^2	-1.56×10^2	1.40×10^2	-7.47×10^1

We first wish to compare the computed performance index from PCIC with the theoretical estimate of Eq. (II-9) to see how closely the linear closed loop dynamics approximates the nonlinear dynamics. The plasma was offset +10 cm and the corresponding state variable vector $\underline{X}_o$ computed. The Plasma-Circuit Interaction Code was then run using the proportional weighted gains and the performance index evaluated by Eq. (II-10). The nominal control voltages were taken from "perfect" feedback simulation. The values of the computed performance index and the theoretical were almost identical, suggesting the viability of the linear model for this phase.

To test whether optimal control gains are optimal in a more complex and nonlinear model, the gains were varied one at a time in PCIC and the performance index with proportional weighting evaluated numerically. The nominal voltages were set to zero, to emphasize the feedback component, and the simulation run through the neutral beam region. Figure 2 shows the variation of performance index with the EF R gain. Both the measurement part of the performance index,

$$\int_{t_o}^{T} (\underline{Y} - \underline{Y}_o)^T Q (\underline{Y} - \underline{Y}_o) dt \quad ,$$

and the total performance index have been plotted. Note that the optimal control theory gain is optimal in PCIC. The minimum falls away quickly, especially for gains greater than twice the optimal. The measurement curve is much flatter, although the theoretical gain is still close to the minimum. The asymmetry in the total curve is due to the increased control authority (oscillations) with large gain.

Figure 3 is a similar plot indicating the behavior of the OH I_p gain. Again, the optimal control theory gain is very near the minimum, but here the

total performance index curve is much flatter than for the EF R gain. The cross gains were also examined in this manner, but they were found to produce extremely flat profiles as might be expected since the position is influenced primarily by the EF and the current primarily by the OH. An exception is the EF $\dot{I}_p$ gain which was flat for small values, but produced large values of the performance index as the gain was increased. This indicates that some of the indirect gains could cause harm to the system if they are too large and little benefit if they are correct! We can conclude that the linear optimal control theory feedback gains are indeed optimal in a more realistic model, but that full state feedback may not be required for "optimal" performance.

A characteristic of linear optimal control which has no analog in classical control is the coupling between the various controlled variables. This comes about by incorporating the coupled system dynamics into the gain matrix, Eq. (II-7). An important question to ask is whether this coupling provides any benefits in a more realistic model. This was examined by giving the plasma an initial +10 cm offset and computing the error in position as a function of time. This hypothetical experiment assumes the limiter is not in place and the plasma can expand freely, conserving toroidal flux. Nominal voltages were taken from "perfect" feedback and both sets of gains were utilized in PCIC as shown in Fig. 4. As would be expected, the proportional weighted gain set is superior to the integral weighted set in bringing the plasma back to its original position. However, when OH feedback is removed, the performance of both sets worsen. Thus, coupling the OH and EF control functions does indeed provide better position control.

To evaluate the feedback during neutral beam heating PCIC was run from the beginning to the end of the phase (just prior to compression) with the nominal voltages set to zero. Figure 5 is a plot of position error, ΔR, as a

function of time for various gains. Note that reasonable control is provided by the proportional weighted set, whereas the integral weighting produces a much larger maximum error and does not even start to control until 40 ms after neutral beams turn on. However, if we preprogram the OH from "perfect" feedback and remove the OH feedback the integral weighted set out-performs the proportional set! Furthermore, if only the EF R gain, OH I_p gain and $\beta_\theta, \dot{\beta}_\theta$ gains are used from the proportional weighting, the results are as good as with full state feedback. Figure 6 is a plot of plasma current error, ΔI_p, as a function of time for the same cases as in Fig. 5. Here it is quite clear that the integral weighted set can not adequately control the plasma current. With the preprogrammed OH, the current is of course almost perfectly controlled (the deviation is due to the discrete control every 1.38 ms used in the real feedback simulation). Again, note that the reduced state feedback provides almost the same control as full state feedback.

The reason for the poor position control with the integral weighted gain set is that the plasma current is not being adequately controlled. It is instructive to consider the OH and EF power supply voltages as a function of time for these cases, Figures 7 and 8 respectively. As can be seen from Fig. 7, the OH voltage from the integral weighted feedback is much too small, compared to the preprogrammed OH, during neutral beam heating. In comparison, Fig. 8 shows the EF voltage from the integral weighted set is quite close to the preprogrammed value from "perfect" feedback. In fact there is not too much difference in the resultant EF voltage from proportional weighted, integral weighted, or "perfect" feedback. We can therefore conclude that to achieve good position control, adequate plasma current control is imperative.

To more fully test the idea that reduced state feedback can be as effective as full state feedback, measurement uncertainty and time delay were

incorporated in the feedback measurements. The uncertainty was provided by assuming the measurements normally distributed about the previously computed values. Every 1.38 ms a new feedback voltage was determined from the Gaussian probability function. Time delay was introduced as a lag between actual measurement and implementation in the feedback. The details are fully discussed in Appendix A. Figure 9 is a plot of ΔR vs. time (corresponding to Fig. 5) with variances of 1 cm in R, 3.5×10^4 amps (5%) in I_p, .3 in β_θ and 6. in $\dot{\beta}_\theta$ (10%). In addition a 2 ms time delay was introduced. The results are similar to Fig. 5 with the exception of the data scatter. Even with noise in the system, reduced state feedback performs as well as full state feedback.

To check the overall quality and sensitivity of the control system, the various gain sets were utilized in PCIC feedback simulation runs to evaluate the proportional weighted performance index as a function of measurement variance, σ. An analysis of the method is presented in Appendix B. Figure 10 is a plot of this performance index J_p vs. $\sigma(R)$ for proportional weighted, integral weighted, and integral weighted with preprogrammed OH. The measurement part of J_p and the total performance index are indicated for each gain set. The difference between the two curves is a measure of how much control authority is required. Figure 10 indicates that the integral weighted set produces the worst overall control, but with preprogrammed OH (and no OH feedback) it produces the best control. The measurement part of J_p from the proportional weighted gains shows good behavior (as could be surmised from Fig. 9) although it starts to degrade more quickly with increasing $\sigma(R)$ than does the integral weighted set's. However, the total performance index for the proportional weighted set is initially large and grows very rapidly with $\sigma(R)$ until it has almost the same value as the index for the integral weighted gains. Thus, the proportional weighted feedback requires considerable control

authority which quickly increases with uncertainty in R. Specifically the EF voltage is oscillating. This is not an attractive mode of control. We would much rather see consistent changes in power supply voltage. The behavior is typical of a higher (proportional) gain system and suggests that in regions where position is poorly determined more integral and less proportional control may be required.

A similar analysis has incorporated measurement uncertainty in I_p as indicated in Fig. 11. In addition to the previous cases an integral weighted preprogrammed EF (with no EF feedback) has been included. It has the worst performance due to its very poor measurement J_p, suggesting feedback is required in order to achieve the tight position (~ 1 cm) control. The preprogramed OH is satisfactory because I_p is less heavily weighted than R in this particular performance index. The big difference in uncertainty dependence is that the integral weighted gains show the most sensitivity to $\sigma(I_p)$. The reason is the poor measurement index behavior. It is the main contribution to the total performance index and is evidence of the poor plasma current control. The total performance index with proportional weighted feedback grows quickly with $\sigma(R)$ because of increasing control authority, whereas the integral weighted J_p increases sharply with $\sigma(I_p)$ because of poor R and I_p control.

Similar sensitivity studies were attempted with uncertainty in $\beta_\theta, \dot{\beta}_\theta$ and time delays. The results were that uncertainty in β_θ and $\dot{\beta}_\theta$ up to 20% and time delays up to 3 ms produced no control degradation. This is a pleasing result since β_θ cannot be accurately measured. It is thus possible to use $\beta_\theta, \dot{\beta}_\theta$ as feedback (instead of feedforward) measurements and utilize good nominal voltage waveforms to anticipate the initial effects of neutral beam heating. The time delay results would give us considerable freedom in

hardware design, but unfortunately only hold true here and in the post-compression phase. Startup is another matter, as will be seen in Section VII. However, the time delay in this region is similar to eddy current effects.[2] Therefore, the control may not be affected too greatly by eddy currents.

It has been previously shown that very good control is possible during neutral beam heating (R within 1 cm, I_p within 5%) using only rough DC nominal voltages.[2] This section has shown that linear optimal control is on a sound basis during this phase of the discharge. In particular, proportional feedback is important to achieve control objectives, but can prove sensitive to measurement uncertainty in R. It would seem best to experiment with gain sets somewhere in between the pure proportional and pure integral. In addition, coupling the OH and EF control does provide the best results whereas full state feedback does not. The last point is significant when including eddy currents in the model. It seems likely that only direct discharge parameters ($I_p, \dot{I}_p, R, \dot{R}$) will be required for feedback measurements. By removing the indirect measurements ($I_{OH}, \dot{I}_{OH}, I_{EF}, \dot{I}_{EF}$) we can protect against imperfect power supply models. For example, the use of the power supply currents as feedback measurements could necessitate a change in voltage even without error in plasma major radius and current, if ΔI_{OH} and ΔI_{EF} were not zero. This is clearly not the way to design a control system. If more measurements are required semi-direct ones such as the difference between the Shafranov and actual I_{EF} should be tried.

VI. Control After Compression

The major control objective after compression is to halt the plasma motion and maintain its position and current. Of course, to brake the plasma

an initial nominal voltage is required. This has been accomplished and is described in detail in Ref. 2. A problem in this phase is that to produce the required B_V a large EF current is required, which drastically limits the EF voltage according to the current-voltage characteristics of the power supplies.[5]

The control gains were determined by utilizing the pre-compression model and linearizing the equations just after compression. The discrete time gains are listed in Table VI-1. The performance index weights were the same as the proportional weighting in pre-compression, Table V-1. The control was evaluated in the PCIC by initially offsetting the plasma position + 10 cm and using nominal voltages from "perfect" feedback. Figure 12 is the position error time history with and without OH feedback. First note the long control time constant compared to the pre-compression region, Fig. 4. This is because the required EF voltage is greater than available for the first 6 ms. The simulation just uses the allowable voltage in these circumstances. The time histories in Fig. 12 are almost identical until the last half of the phase. Here the coupled feedback settles down to the desired major radius while that without OH feedback retains a 0.5 cm error for 10 ms before starting slowly downward. The final plasma current is 3% too high with OH feedback and 10% too high without. Figure 13 is a similar time history but with measurement uncertainty and time delay [$\sigma(R)$ = .01 m, $\sigma(I_p)$ = 3.5 x 10^4 amps, time delay = 2 ms]. As can be seen from the plot, the position control is about the same whether OH feedback is included or not.

The sensitivity to measurement uncertainty is examined in Figs. 14 and 15 where the evaluated performance index is plotted as a function of $\sigma(R)$ and $\sigma(I_p)$ respectively. Figure 14 indicates a small preference for including OH feedback, although both indices increase at about the same rate as $\sigma(R)$ increases. Also both required significantly more control authority as $\sigma(R)$

Table VI-1

Post-Compression Discrete Feedback Gains

	EF	OH
R	2.94×10^{5}	2.97×10^{4}
$\dot{I}_p$	-6.55×10^{-4}	-1.36×10^{-4}
I_p	-1.47×10^{-2}	-8.61×10^{-2}
$\int Rdt$	0.	0.
$\int Ipdt$	0.	0.

becomes greater than 1 cm. Figure 15 shows that again measurement control is somewhat better when OH feedback is included. However, its control authority increases much faster with increasing $\sigma(I_p)$ than does the solely EF feedback. The reason is that the OH voltage begins to oscillate when OH feedback is included and $\sigma(I_p)$ increases (greater than 3.5%).

The post-compression feedback shows a slight preference for coupled OH and EF control. However, if the measurements are noisy this may not be true. In particular, uncertainty in plasma current may cause an oscillating OH voltage. This would indicate that the proper performance index weighting should be in between pure proportional and pure integral, at least for I_p. Since the OH feedback contributes little to the position control, except for the small DC error, it may even prove worthwhile to consider integral weighting for I_p and proportional weighting for R.

VII. Control During Startup

Startup poses its own special control problems with an expanding plasma and rapidly increasing current. The objective is to increase the plasma

current while maintaining the safety factor, q, ~ 3 at the limit [5] This condition then specifies the growth rate. The plasma is grown off the limiter in order to minimize skin currents. Eddy currents will be extremely important during startup, at least for the first 10 ms. Thus, the feedback gains derived in this section would be suspect for actual use in this region.

Since the OH rectifier does not become active until well into startup[5] (initially a large preset OH current is commutated across an external resistor), the OH circuit was not included in the linear model. As mentioned in Section III, startup incorporates a growth model, a + R = constant, instead of the toroidal flux conservation used in the other regions of the discharge. The plasma internal inductance, $\ell_i/2$, has been assumed to be constant and equal to 0.5. This is not correct during early startup, but since the current penetrates the initially small plasma (a_o = 20 cm) within a few milliseconds[5] it is a reasonable assumption. Also current penetration was not utilized in PCIC for the startup runs, to avoid numerical sensitivities. A more detailed examination with eddy currents included would justify the current penetration dynamics. Of course, realistically the first several milliseconds will be beyond the scope of active feedback control and accurate preprogramming will be necessary for discharge initiation.

The state variables in the startup model are I_p and I_{EF} with the measurement set R and $\dot{R}$. The derivative of major radius can now be utilizied since I_{OH} does not have to be expressed in terms of the measurements. The performance index weights and EF gains are listed in Table VII-1. Again the discrete gains are indicated with a sample time of 1.38 ms.

The EF gains were first tested for optimality in PCIC by varying the $\dot{R}$ gain and evaluating the performance index, Fig. 16. For all of the startup runs nominal voltages were taken from "perfect" feedback results. Figure 16

shows that again the linear optimal control theory gains are optimal in the more realistic model. Furthermore, both the measurement and total performance index form very sharp minima, indicating there is very little room for error in choosing this gain. A similar test of the R gain provided almost no dependence. Apparently only the $\dot{R}$ gain is significant because of the very fast rise in plasma current which then sets the rate for growth. With a much slower current buildup the R gain might attain some significance.

Table VII-1

Performance Index Weights and Discrete

EF Feedback Gains During Startup

	Weights	EF Gain
R	10^3	6.1×10^2
$\dot{R}$	10^{-1}	58.5
V_{EF}	10^{-5}	

To test the actual control, a time history of the safety factor, q, was evaluated at the limiter in feedback simulation with and without an initial + 10 cm offset, Fig. 17. Here the limiter does come into play as it reduces the plasma minor radius according to the growth model. The desired q(a) is 3.0, and its deviation without an initial offset is due to the discrete control. The recovery from a +10 cm offset takes about 20 ms and still does not fully return to the desired q value. This points to the difficulty of control during startup.

The feedback sensitivity to measurement uncertainty and time delay is shown in Fig. 18 where the PCIC evaluated performance index is plotted as a function of $\sigma(R)$, $\sigma(\dot{R})$, and time delay. Measurement uncertainty in R is not very significant, but the performance index rises very sharply with $\sigma(\dot{R})$. The total performance index is dominated by the measurement part indicating that there is no way to control the plasma position when measurement of $\dot{R}$ becomes poor. This should be taken into account when considering magnetic loop measurements of $\dot{R}$ since eddy currents can make them very noisy. On the other hand time delay does play an important role during startup, but primarily by increasing control authority. There is an initial degradation in control as a time delay of 1 ms is introduced, but it gets no worse as the delay stretches to 3 ms. However, the total performance index climbs very quickly as the time delay increases. We may be able to maintain position with time delays greater than 1 ms, but at the expense of very demanding power supply operation. Again, note that time delay may simulate eddy current effects by introducing a lag in applied control voltage.

Startup will pose significant control problems due to eddy currents, discrete control, and measurement uncertainty. It appears that a reduced measurement set will perform satisfactorily as only $\dot{R}$ is important when the plasma current is quickly built up. A heavy reliance on accurate preprogramming will definitely be required.

VIII. Control During Termination

During termination the objective is to maintain the plasma position as the plasma current is quickly decreased by reversing the OH current. Therefore, we need only concern ourselves with control of the EF power supply. The measurement set $R, I_p, \dot{I}_p, \int R dt$ has been utilized in this region and Table VIII-1 lists the gains.

The position control was tested by initially offsetting R by +10 cm and evaluating the position error, ΔR, time history, Fig. 19. Nominal voltages were taken from "perfect" feedback. The error comes down to zero within 10 ms, but then overshoots to 2 cm. From here the error is smoothly and gradually (15 ms) brought to zero without further oscillation. With a -10 kV nominal DC EF voltage and no initial offset the maximum error is + 2 cm and the average less than 0.5 cm. During this phase the EF voltage ranges from -8.8 kV to -1.4 kV in the "perfect" feedback simulation, so active feedback is significant. These results are within design criteria and could of course be improved by a time varying nominal voltage.

Table VIII-1

Discrete EF Feedback Gains During Termination

R	2.1×10^{5}
$\dot{I}_p$	3.3×10^{-4}
I_p	2.4×10^{-3}
$\int R dt$	2.5×10^{7}

PCIC Simulation Weights

R	$1. \times 10^{4}$
I_p	$1. \times 10^{-9}$
V_{EF}	$1. \times 10^{-7}$

The sensitivity of the feedback to measurement uncertainty and time delay is indicated in Fig. 20 where the PCIC evaluated performance index dependence on $\sigma(R)$, $\sigma(I_p)$, and time delay is plotted. Time delay has little effect on the achievable control, but does contribute to control authority. However, increasing the time delay from 1 ms to 3 ms has minor consequences. Measurement uncertainty in R and I_p causes similar increases in both the measurement and total performance index, with the increase especially sharp after the variance is doubled. Somewhat more control authority is required for the same measurement control with uncertainty in R as opposed to I_p. This effect is also much greater as the variance doubles.

The heavily integral flavored control used in this example provides a smooth and accurate feedback strategy. While measurement uncertainty does cause control degradation, it is only significant for a large variance. The control authority is more substantial, but the performance index is still quite low even accounting for the weighting of only one power supply. Time delay is not too significant which may indicate that eddy current effects will not greatly alter the gains. However, this must be taken with caution since eddy currents will be strongly excited by the other rapidly changing currents.

IX. Conclusions

The major objective of this work has been to evaluate the use of modern optimal control theory for active feedback control of plasma position and current in TFTR. For simplicity eddy currents were not considered in the present study. It has been shown that by breaking the discharge into discrete segments appropriate linear models and control gains can be developed. Furthermore, methods for analyzing the control by evaluating the performance index in the Plasma-Circuit Interaction Code have been presented. This

provides an independent and physical means for understanding feedback in a realistic model. By introducing experimental uncertainties into the simulation, control quality and sensitivities have been studied. Finally, the assumptions and predictions of linear optimal control theory have been tested in a nonlinear model which incorporates effects either simplified or ignored in the linear control models.

The results of the above procedures are:

1. The linear model provides a good description of the closed loop dynamics, especially during pre-compression and neutral beam heating.
2. Linear optimal control gains are "optimal" in the nonlinear and more realistic Plasma-Circuit Interaction Code.
3. Accurate plasma position control requires good plasma current control.
4. Better position control is generally achieved by coupling the OH and EF feedback.
5. Full state feedback is not required for either performance or stability. This bodes well for eddy current inclusion as the direct discharge parameters should suffice for feedback measurements.
6. Measurement uncertainty up to 20% in β_θ and $\bar{\beta}_\theta$ does not affect the control. Also time delays up to 3 ms were insignificant during pre- and post-compression, but were important in startup and termination.
7. Considerable control authority (and voltage oscillation) can occur with high proportional gains and measurement uncertainty. Conversely, low proportional gains are less

sensitive but may not provide accurate control. In practice the whole gain spectrum, in between the extremes considered here, should be evaluated according to actual experimental conditions.

ACKNOWLEDGMENTS

I would like to acknowledge the many helpful discussions concerning this work with L. Michaels of PPPL, and R. Gran and M. Rossi of the Grumman Aerospace Corporation.

This work was supported by U.S. Department of Energy Contract No. DE-AC02-76-CHO-3073.

Appendix A - Feedback in the Plasma-Circuit Interaction Code

The basic circuit equations and the differentiated Shafranov equation are fully described in Appendix A of Ref. 5. Both the feedback and "perfect" feedback modes of operation use the same system of equations. The difference is that "perfect" feedback incorporates discharge constraints in solving for the variables, which include power supply voltages. The feedback mode accepts the power supply voltages as input and solves the system of equations for $\dot{\underline{I}}$ and $\dot{R}$. These are then integrated to get the current vector and major radius. The vector $\underline{I}$ includes OH, EF, total plasma, internal plasma (for $\ell_i/2$), and eddy currents.

The power supply voltages are determined from

$$\underline{V} = \underline{V}_o + G(\underline{Y} - \underline{Y}_o) \quad , \tag{A-1}$$

where $\underline{V}_o$ are the nominal OH and EF voltages.

G is the gain matrix.

$\underline{Y}$ are the values of the feedback measurements.

$\underline{Y}_o$ are the desired measurement values.

Measurement uncertainty is introduced in $\underline{Y}$ by

$$\underline{Y} = \underline{Y}_c + \underline{\sigma}\, U \quad , \tag{A-2}$$

where $\underline{Y}_c$ is the present value of the measurement from the integrated system dynamics.

$\underline{\sigma}$ is the variance vector.

U is a randomly determined value of the normalized error function.

The measurements are thus assumed to be normally distributed about the present value $\underline{Y}_c$. The $\underline{Y}$ are only used in the feedback portion of the code to compute feedback voltages. The integrated system variables are always the $\underline{Y}_c$. Time delay is introduced into the system by saving past values of the measurements and utilizing them in Eq. (A-1). The magnitude of the time delay determines which of the past values is taken. Since the previous measurements are stored in arrays at fixed time intervals, interpolation is used to provide an estimate of the measurement at the requested time. Again, these past values of $\underline{Y}_c$ are only used in the feedback portion of the code in order to determine feedback voltages.

Appendix B - Analysis of Measurement Uncertainty in the Performance Index

The effect of measurement uncertainty on the PCIC evaluated performance index provides significant information on the quality of feedback control. This process will be examined in more detail to indicate the influence of the relevant parameters. If $\underline{n}(t)$ denotes an uncertainty vector corresponding to the measurement $\underline{Y}_c$ vector we can express the measurement and control perturbation as

$$\underline{\tilde{Y}} = \underline{\tilde{Y}}_c + \underline{n} \quad , \; E\{\underline{n}\} = 0, \text{ and } E\{\underline{n}^T\underline{n}\} = \sigma^2 \tag{B-1}$$

$$\underline{\tilde{u}} = G^T\underline{\tilde{Y}} = G^T\underline{\tilde{Y}}_c + G^T\underline{n}$$

where: $\underline{\tilde{Y}}_c = \underline{Y}_c - \underline{Y}_o$.

$$\underline{\tilde{u}} = \underline{u} - \underline{u}_o$$

The total performance index is now from Eq. (II-10)

$$J = \int_{t_o}^{T} \left\{ (\underline{\tilde{Y}}_c + \underline{n})^T Q (\underline{\tilde{Y}}_c + \underline{n}) + (G^T\underline{\tilde{Y}}_c + G^T\underline{n})^T R (G^T\underline{\tilde{Y}}_c + G^T\underline{n}) \right\} dt. \tag{B-2}$$

Transforming to the discrete computation performed in PCIC we can make the following identifications:

$$\Sigma \underline{Y}_c^T \tilde{Q} \underline{Y}_c \Delta t = J_M \ (\sigma = 0) \tag{B-2}$$

$$\Sigma (\underline{n}^T \tilde{Q} \underline{n} + 2 \underline{Y}_c^T \tilde{Q} \underline{n}) \Delta t = J_M(\sigma) - J_M \ (\sigma = 0) \tag{B-3}$$

$$\Sigma (\underline{Y}_c^T \tilde{Q} \underline{Y}_c + \underline{Y}_c^T G \tilde{R} G^T \underline{Y}_c) \Delta t = J \ (\sigma = 0) \tag{B-4}$$

$$\Sigma (\underline{n}^T G \tilde{R} G^T \underline{n} + 2 \underline{Y}_c^T G \tilde{R} G^T \underline{n}) \Delta t =$$

$$J(\sigma) - J(\sigma = 0) - \left[J_M(\sigma) - J_M(\sigma = 0)\right] \tag{B-5}$$

where: J_M = measurement part of the performance index.

$J(\sigma)$ = performance index with variance σ.

$\underline{Y}_c$, $\underline{n}$ are functions of time.

From Eq. (B-3) we can express Eq. (B-5) as

$$\left(\frac{\tilde{R} G^T}{Q_n}\right) \Sigma (2 \underline{Y}_c^T + \underline{n}^T) \tilde{Q} \underline{n} \Delta t = J(\sigma) - J(\sigma = 0) - [J_M(\sigma) - J_M(\sigma = 0)] \tag{B-6}$$

since G, $\tilde{R}$, $\tilde{Q}$ are constant matrices and $\tilde{Q}\underline{n}$ will collapse to a single value, Q_n, once the matrix multiplication is carried out, if only one component of $\underline{n}$ is considered at a time. This is in fact done in the simulation tests of J_p vs σ.

These expressions can be tested with the values of the performances index during pre-compression from Figs. 10 and 11. This procedure is only valid for the proportional weighted gain set, since the performance index computed in PCIC only contains proportional weights independent of the actual derived gain set. The performance index values are:

	$J_M(\sigma) - J_M\ (\sigma = 0)$	$J(\sigma) - J(\sigma = 0) - [J_M(\sigma) - J_M(\sigma = 0)]$
$\sigma(R) = .02$	1.3	0.4
$\sigma(I_p) = 7 \times 10^4$	0.9	0.7

and $$\left(\frac{G\,\tilde{R}\,G^T}{Q_n}\right) = \begin{cases} .27 \text{ for } \sigma(R) \\ .65 \text{ for } \sigma(I_p) \end{cases}$$

Multiplying the values of $J_M(\sigma) - J_M(\sigma = 0)$ by the respective $(\tilde{GRG}^T/Q_n)$ quantity does give values very close to those determined from the actual evaluation in PCIC.

References

1. R. Gran, M. Rossi, and F. Sobierajski, Proceedings of the 7th Symp. on Eng. Probs. of Fusion Research, Knoxville; IEEE No. 77CH1267-4-NPS, pp. 104-111, Oct. 1977.

2. R. Gran, M. Rossi, and M. Firestone, Proceedings of the 8th Symp. on Eng. Probs. of Fusion Research, San Francisco; IEEE No. 79CH1447-5 NPS, pp. 1854-1862, Nov. 1979.

3. A. Ogata and H. Ninamiya, Proceedings of the 8th Symp. on Eng. Probs. of Fusion Research, San Francisco; IEEE No. 79CH1441-5 NPS, pp. 1879-1883, Nov. 1979.

4. K. Fukunishi, S. Saito, A. Ogato, and H. Minomiya, Japanese Journal of Applied Physics, Vol. 19, No. 9, pp. 1729-1736, Sept. 1980.

5. R. J. Hawryluk, M. A. Firestone, U. R. Christensen, H. Fishman, and J. A. Schmidt, TFTR Physics Group Report #29, Princeton Plasma Physics Laboratory, June 1980.

6. H. Kwakernak and R. Sivan, Linear Optimal Control Systems, Wiley-Interscience, New York, 1972.

7. M. J. Rossi, Grumman Research Control Theory Library-CONTHE, to be published as a Grumman Research Report.

8. U. S. Mukhovatov and V. B. Shafranov, Nucl. Fusion 11, (1971) 605.

FIGURE CAPTIONS

Figure 1 — Above the plasma electron and ion temperature and β_θ time histories for the strong compression discharge. Below is the plasma major radius and current time history for the discharge. Neutral beams are on from .24 to .29 sec with compression immediately following.

Figure 2 — The variation in measurement and total proportional weighted performance index as a function of the EF R gain for pre-compression. The optimal control theory gain is indicated.

Figure 3 — The variation in measurement and total proportional weighted performance index as a function of the OH I_p gain for pre-compression. The optimal control theory gain is indicated.

Figure 4 — Position error time history for feedback with proportional and integral weighted gains during pre-compression with and without OH feedback. Nominal voltages were taken from "perfect" feedback. The plasma was initially offset +10 cm.

Figure 5 — Position error time history during pre-compression and neutral beam heating. The nominal voltages were set to zero. Feedback with proportional and integral (with and

without OH feedback) weighted gains. Also feedback with only proportional weighted EF R, OH Ip, β_θ, $\hat{\beta}_\theta$ gains.

Figure 6 Plasma current error time history for the cases in Figure 5.

Figure 7 OH power supply voltage time history for the cases in Figure 5.

Figure 8 EF power supply voltage time history for the cases in Figure 5.

Figure 9 Position error time history corresponding to cases in Figure 5 but with measurement variances of 1 cm in R, 3.5 x 10^4 amps (5%) in I_p, 0.3 in β_θ and 6.0 in $\hat{\beta}_\theta$ (10%). Also included is a time delay of 2 ms.

Figure 10 The measurement and total proportional weighted performance index variation with $\sigma(R)$ during pre-compression. Feedback with proportional and integral (with and without preprogrammed OH) weighted gains.

Figure 11 The performance index variation with $\sigma(Ip)$ for the cases in Fig. 10. Additionally OH feedback for integral weights and preprogrammed EF is shown.

Figure 12 Position error time history after compression, with and without OH feedback. The nominal voltages were taken from "perfect" feedback.

Figure 13 Position error time history as in Fig. 11, but with measurement variances of 1 cm in R, 3.5×10^4 amps in I_p and a time delay of 2 ms.

Figure 14 The measurement and total performance index variation with $\sigma(R)$, with and without OH feedback, after compression.

Figure 15 The measurement and total performance index variation with $\sigma(I_p)$, with and without OH feedback, after compression.

Figure 16 The variation in measurement and total performance index with the EF $\dot{R}$ gain during start up. The optimal control theory gain is indicated.

Figure 17 The safety factor, q, evaluated at the limiter during start up. Feedback with and without an initial +10 cm offset is shown. The nominal voltages were taken from "perfect" feedback.

Figure 18 The measurement and total performance index variation with $\sigma(R)$, $\sigma(\dot{R})$ and time delay during start up.

Figure 19 The position error time history for feedback during termination. The plasma was given an initial +10 cm offset and the nominal voltages were taken from "perfect" feedback.

Figure 20 The measurement and total performance index variation with $\sigma(R)$, $\sigma(I_p)$, and time delay during termination.

81P0160

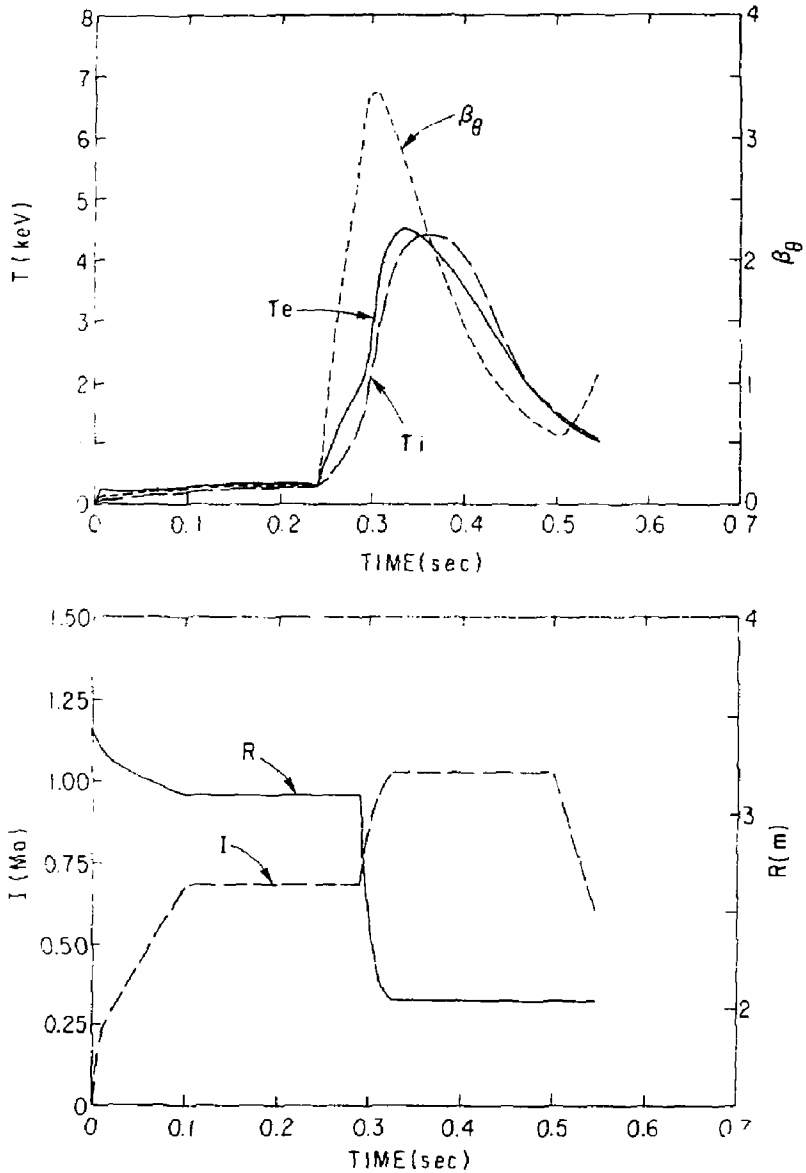

Fig. 1

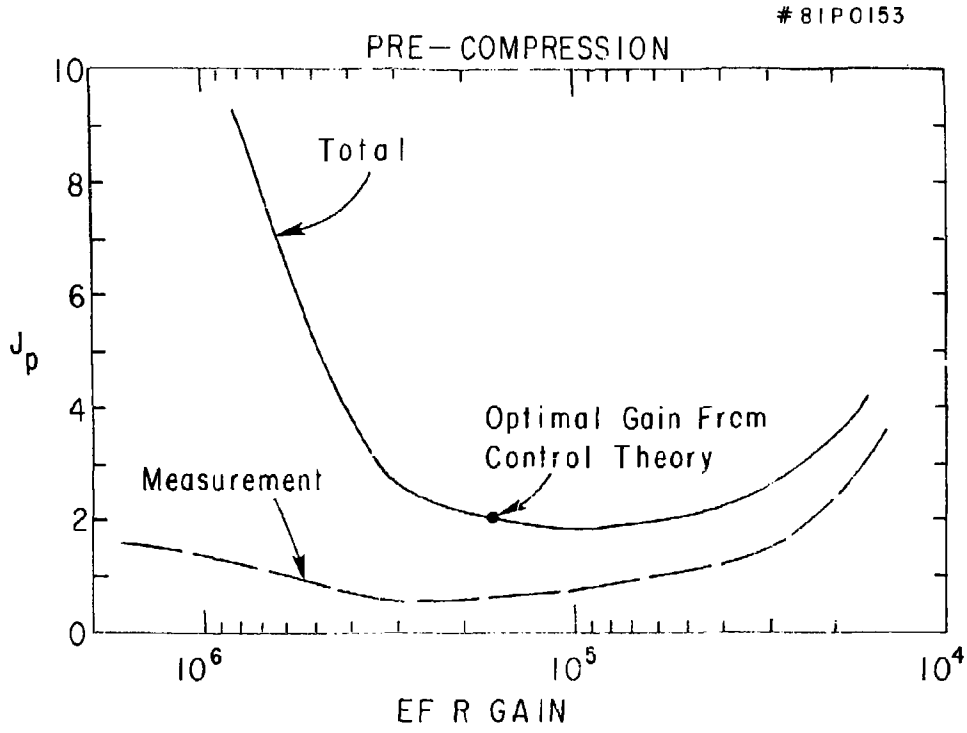
#81P0153
PRE—COMPRESSION
10
8
6
4
2
0
J_p
Total
Optimal Gain From
Control Theory
Measurement
10^6
10^5
10^4
EF R GAIN

FIG. 3

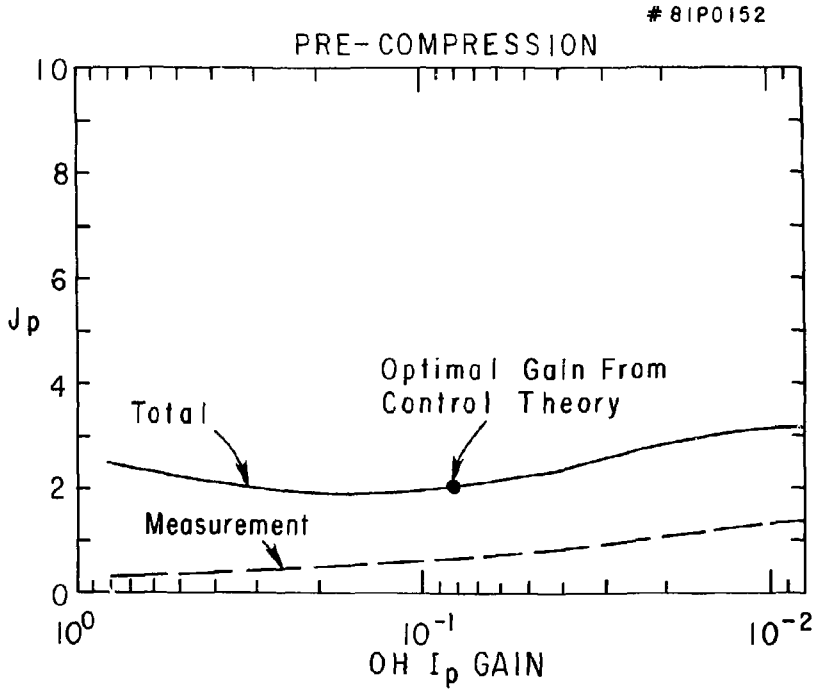
#81P0152
PRE-COMPRESSION
10
8
6
4
2
0
Jp
Optimal Gain From
Control Theory
Total
Measurement
10^0
10^{-1}
10^{-2}
OH I_p GAIN

Fig. 3

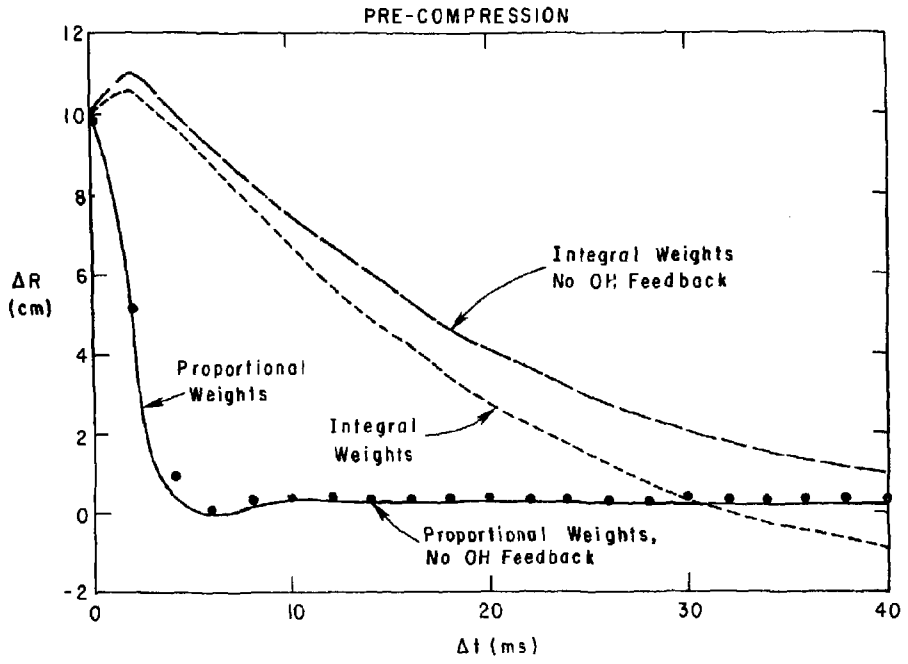
PRE-COMPRESSION
ΔR (cm)
Δt (ms)
Integral Weights No OH Feedback
Proportional Weights
Integral Weights
Proportional Weights, No OH Feedback
12
10
8
6
4
2
0
-2
0
10
20
30
40

Fig. 4

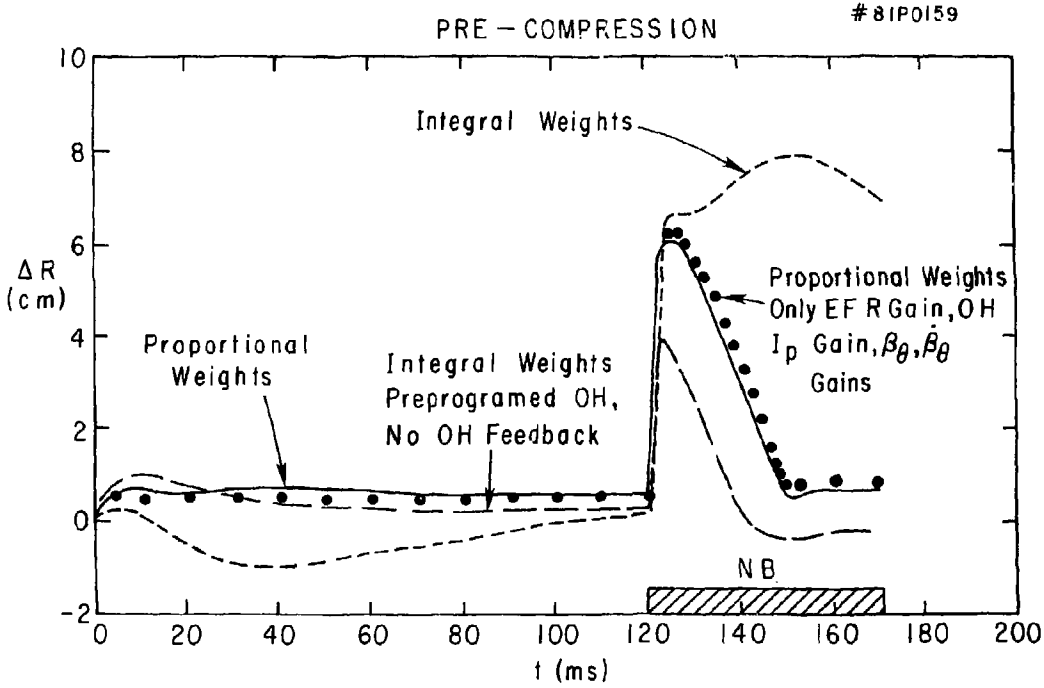
PRE – COMPRESSION
#81P0159
Integral Weights
Proportional Weights
Only EF R Gain, OH
I_p Gain, β_θ, $\dot{\beta}_\theta$
Gains
Proportional
Weights
Integral Weights
Preprogramed OH,
No OH Feedback
NB
ΔR
(cm)
t (ms)
10
8
6
4
2
0
-2
0
20
40
60
80
100
120
140
160
180
200

Fig. 5

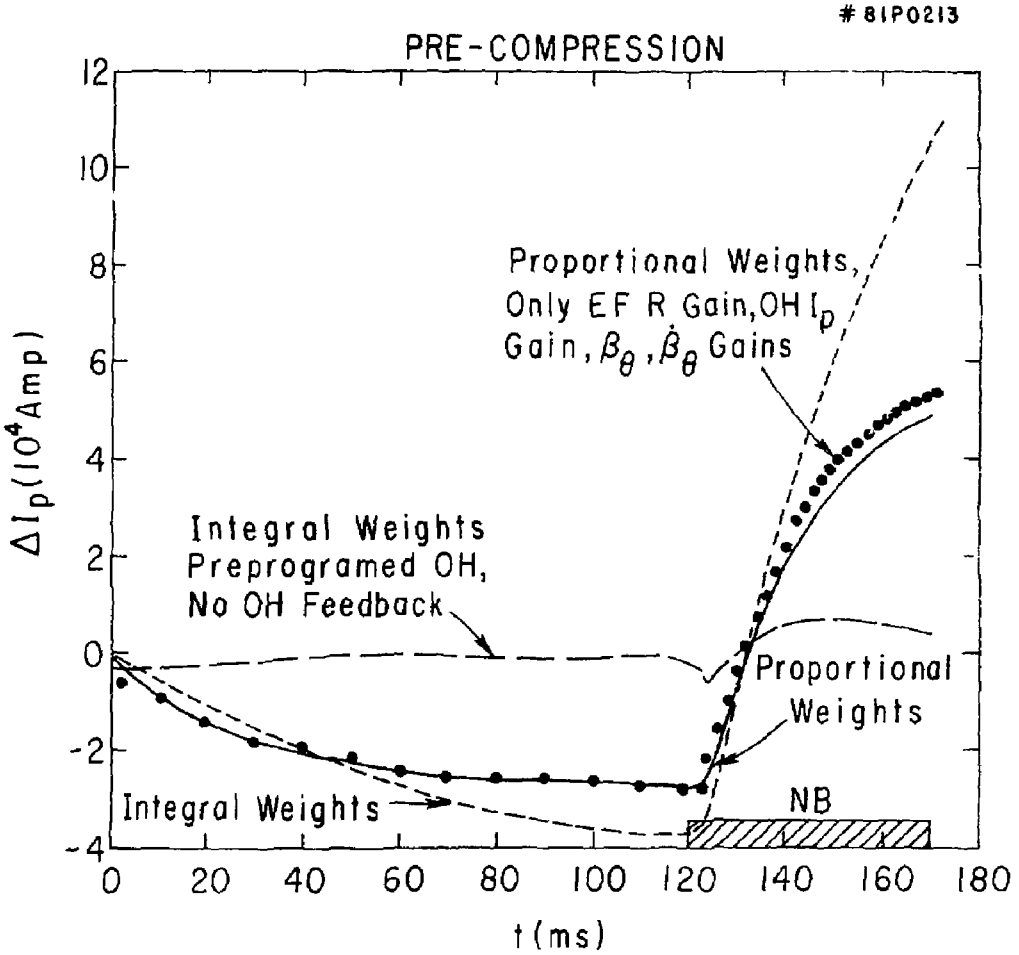
#81P0213
PRE-COMPRESSION
Proportional Weights,
Only EF R Gain, OH I_p
Gain, β_θ, $\dot{\beta}_\theta$ Gains
Integral Weights
Preprogramed OH,
No OH Feedback
Proportional
Weights
Integral Weights
NB
$\Delta I_p (10^4 Amp)$
t (ms)
12
10
8
6
4
2
0
-2
-4
0
20
40
60
80
100
120
140
160
180

Fig. 6

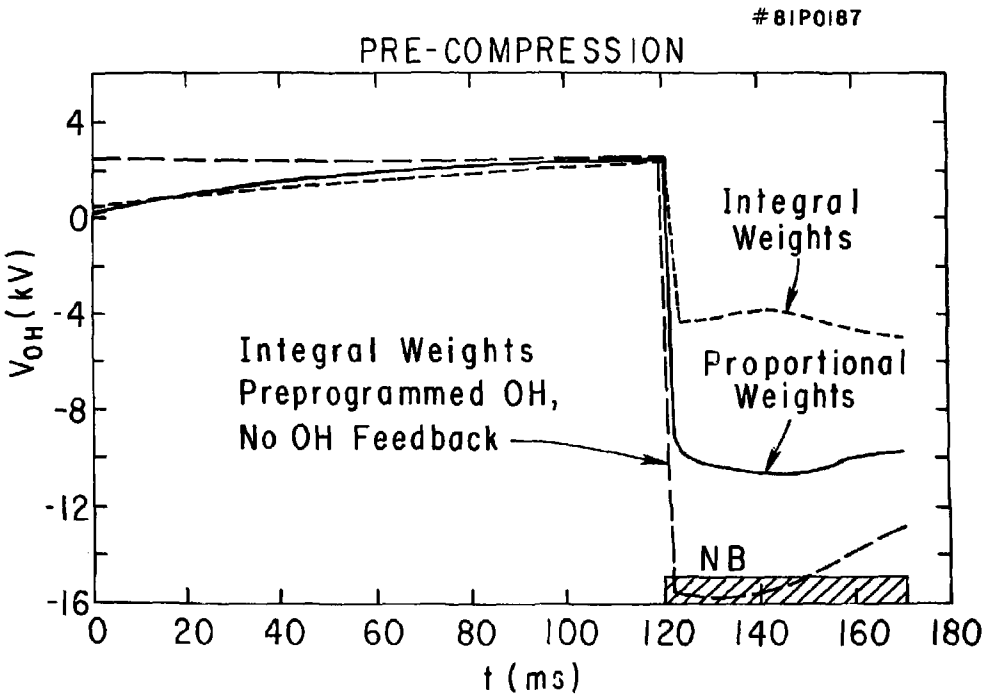
#81P0187
PRE-COMPRESSION
4
0
-4
-8
-12
-16
V_{OH} (kV)
0
20
40
60
80
100
120
140
160
180
t (ms)
Integral Weights
Integral Weights
Preprogrammed OH,
No OH Feedback
Proportional Weights
NB

Fig. 7

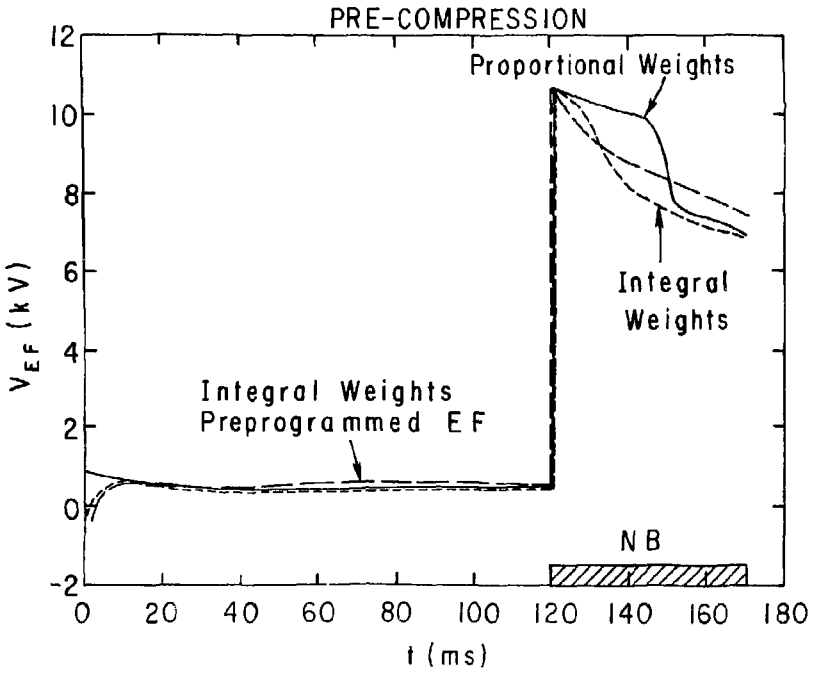
PRE-COMPRESSION
Proportional Weights
Integral Weights
Integral Weights
Preprogrammed EF
NB
V_{EF} (kV)
t (ms)
12
10
8
6
4
2
0
-2
0
20
40
60
80
100
120
140
160
180

Fig. 8

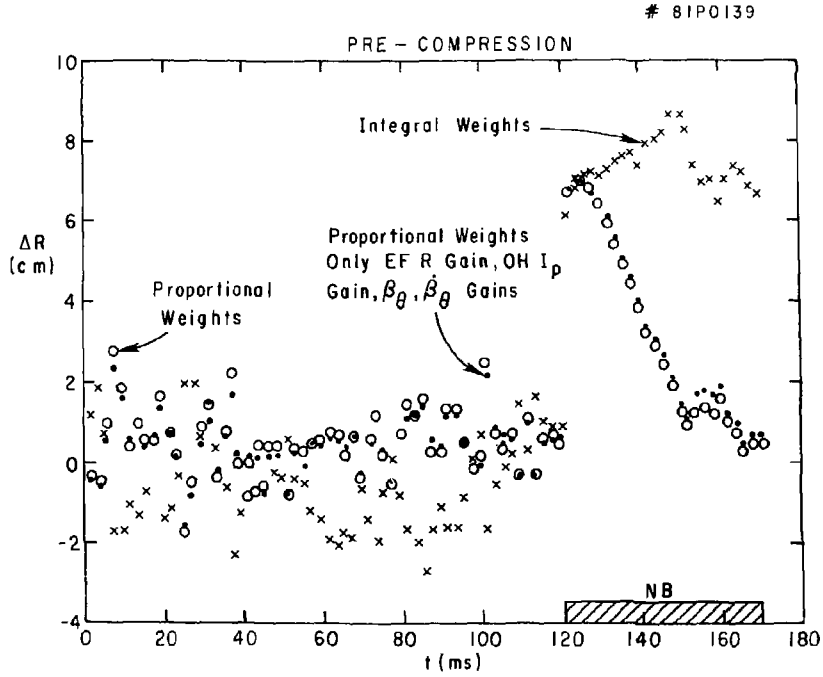
81P0139
PRE – COMPRESSION
Integral Weights
Proportional Weights
Only EF R Gain, OH I_p
Gain, β_θ, $\dot{\beta}_\theta$ Gains
Proportional
Weights
ΔR
(cm)
NB
t (ms)
10
8
6
4
2
0
-2
-4
0
20
40
60
80
100
120
140
160
180

Fig. 9

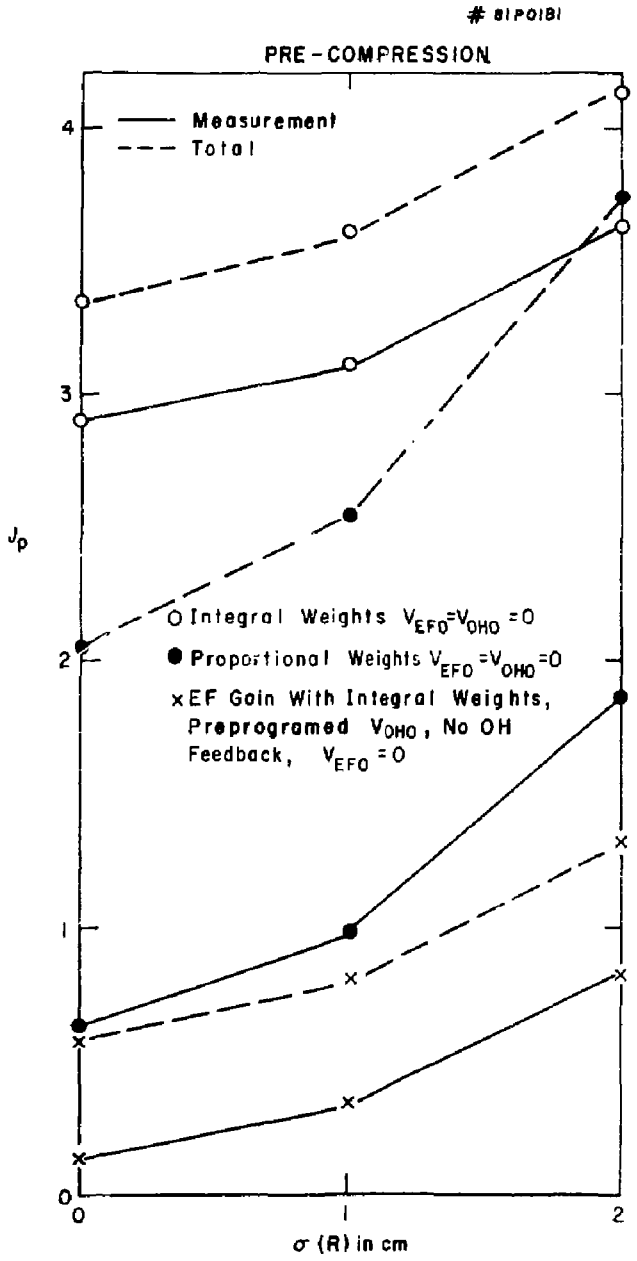
81P01B1
PRE-COMPRESSION
Measurement
Total
J_p
O Integral Weights $V_{EFO}=V_{OHO}=0$
● Proportional Weights $V_{EFO}=V_{OHO}=0$
× EF Gain With Integral Weights, Preprogramed V_{OHO}, No OH Feedback, $V_{EFO}=0$
0
1
2
3
4
σ (R) in cm

Fig. 10

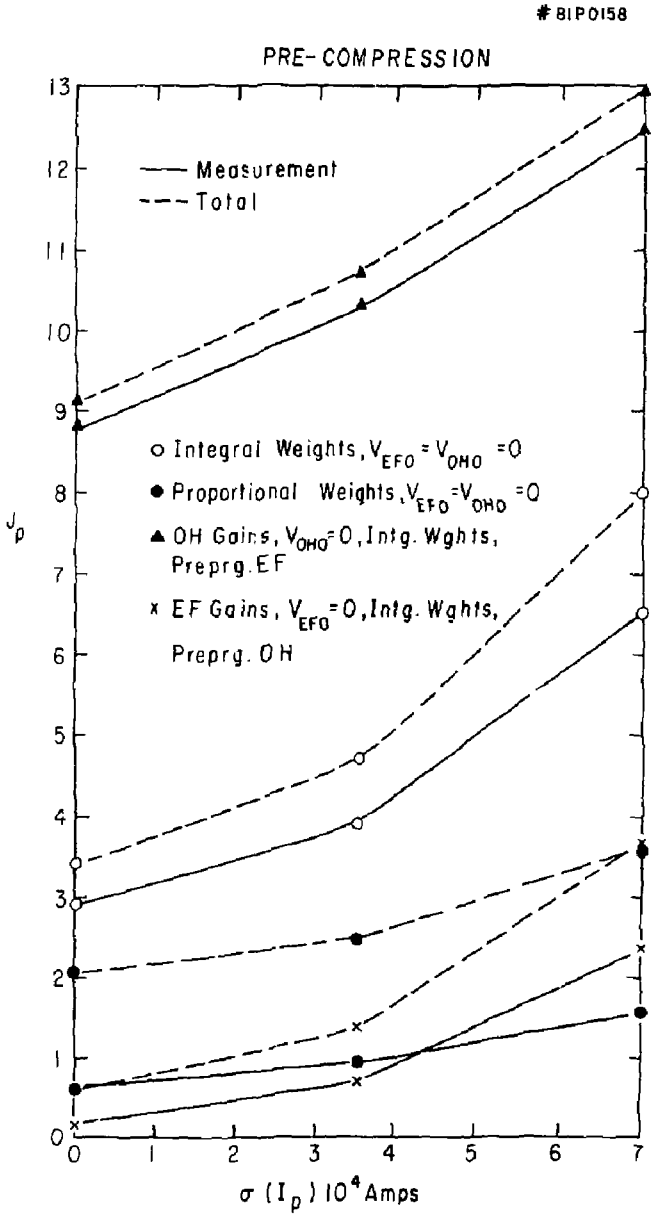
#BIP0158
PRE-COMPRESSION
Measurement
Total
Integral Weights, $V_{EFO} = V_{OHO} = 0$
Proportional Weights, $V_{EFO} = V_{OHO} = 0$
OH Gains, $V_{OHO} = 0$, Intg. Wghts, Preprg. EF
EF Gains, $V_{EFO} = 0$, Intg. Wghts, Preprg. OH
J_p
$\sigma (I_p)\ 10^4$ Amps
0
1
2
3
4
5
6
7
8
9
10
11
12
13

Fig. 11

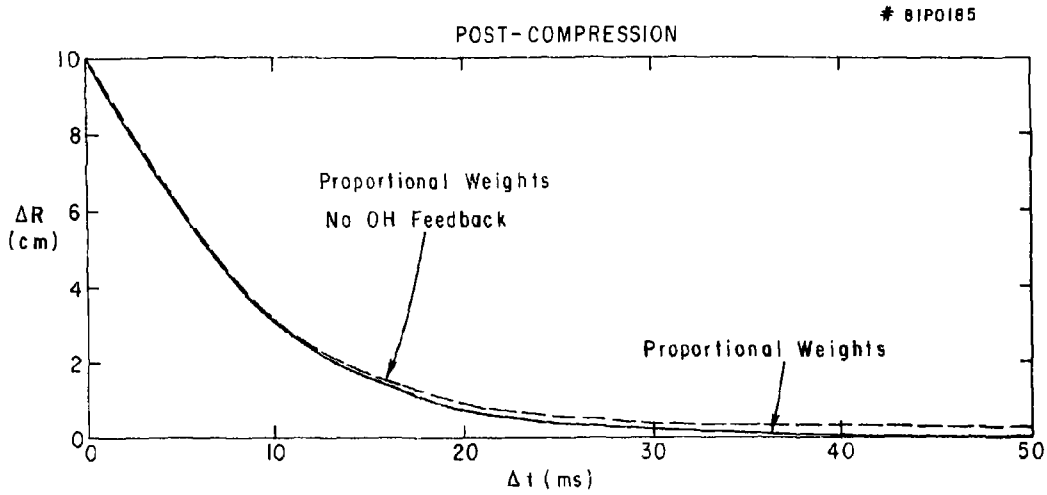
81P0185
POST-COMPRESSION
ΔR (cm)
Δt (ms)
Proportional Weights
No OH Feedback
Proportional Weights
0
2
4
6
8
10
0
10
20
30
40
50

Fig. 12

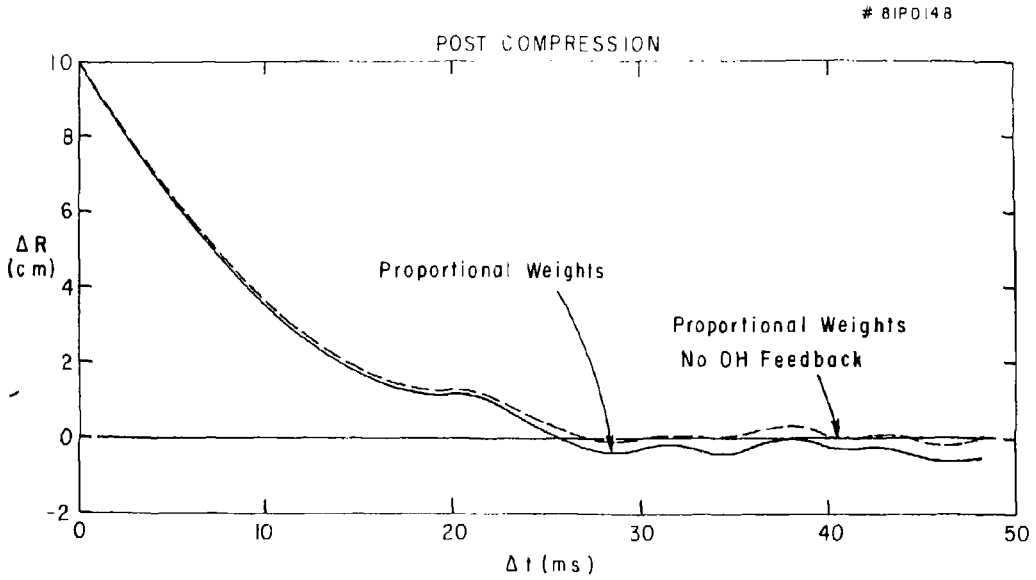
81P0148
POST COMPRESSION
10
8
6
4
2
0
-2
ΔR
(cm)
Proportional Weights
Proportional Weights
No OH Feedback
0
10
20
30
40
50
Δt (ms)

Fig. 13

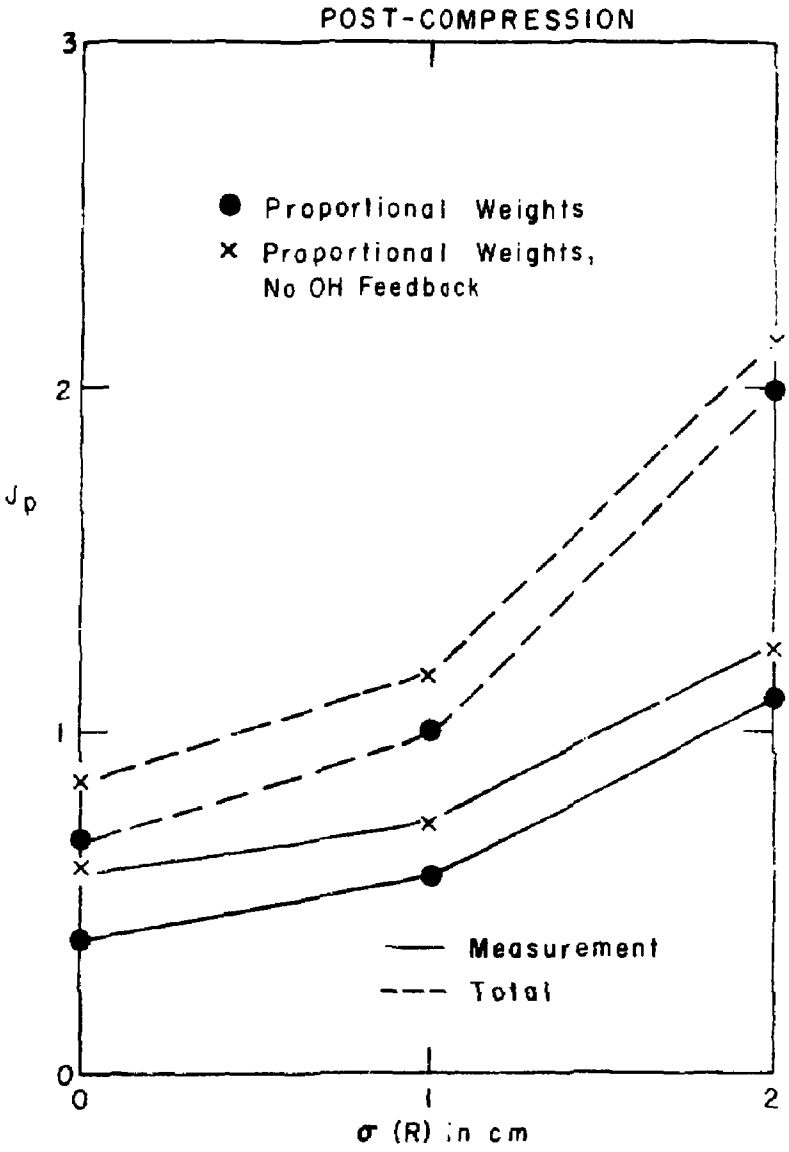

Fig. 14

81P0157

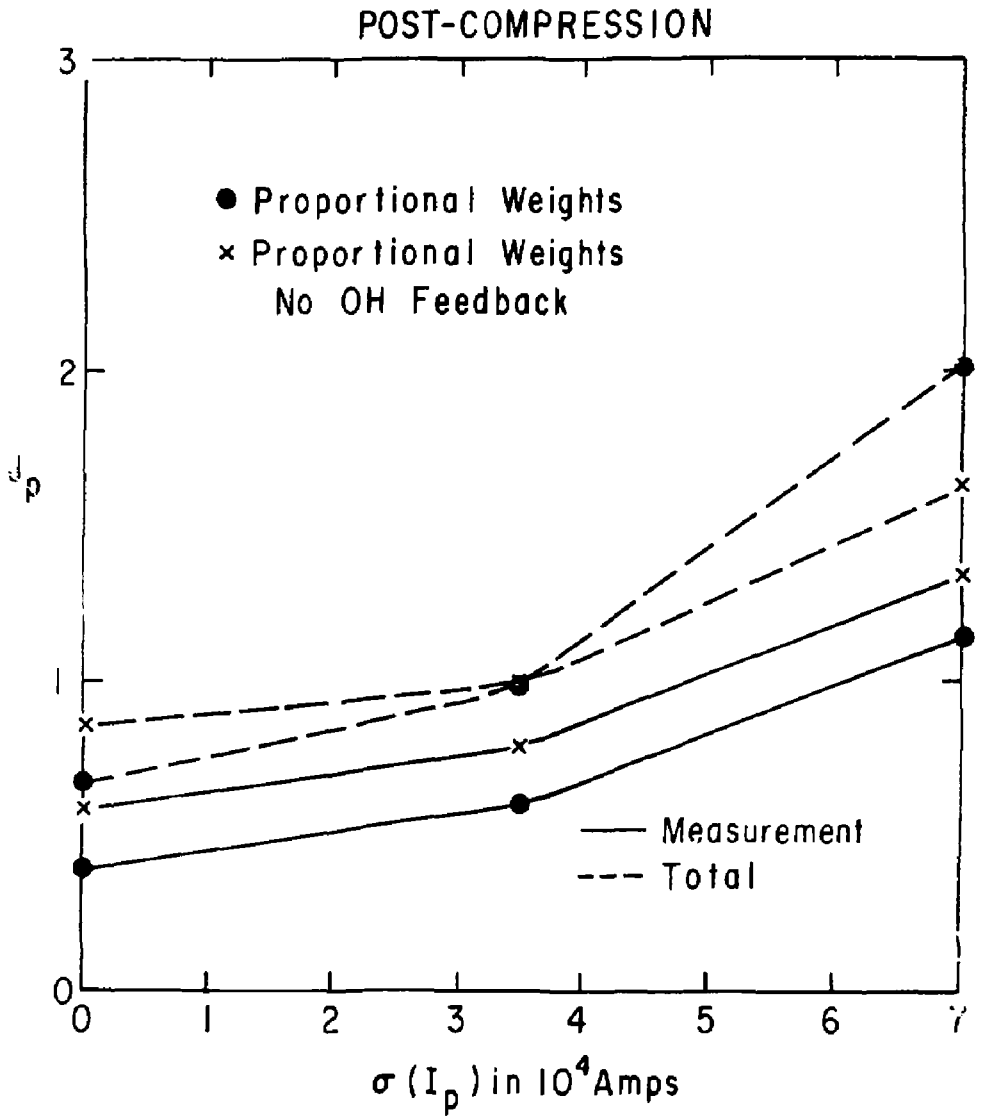

Fig. 15

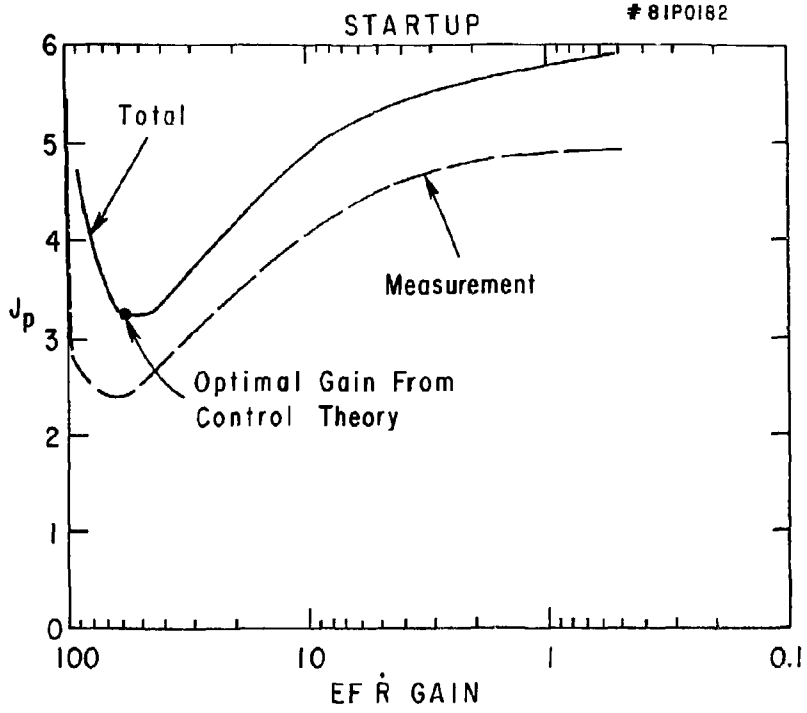
STARTUP
81P0162
Total
Measurement
Optimal Gain From
Control Theory
J_p
6
5
4
3
2
1
0
100
10
1
0.1
EF $\dot{R}$ GAIN

Fig. 16

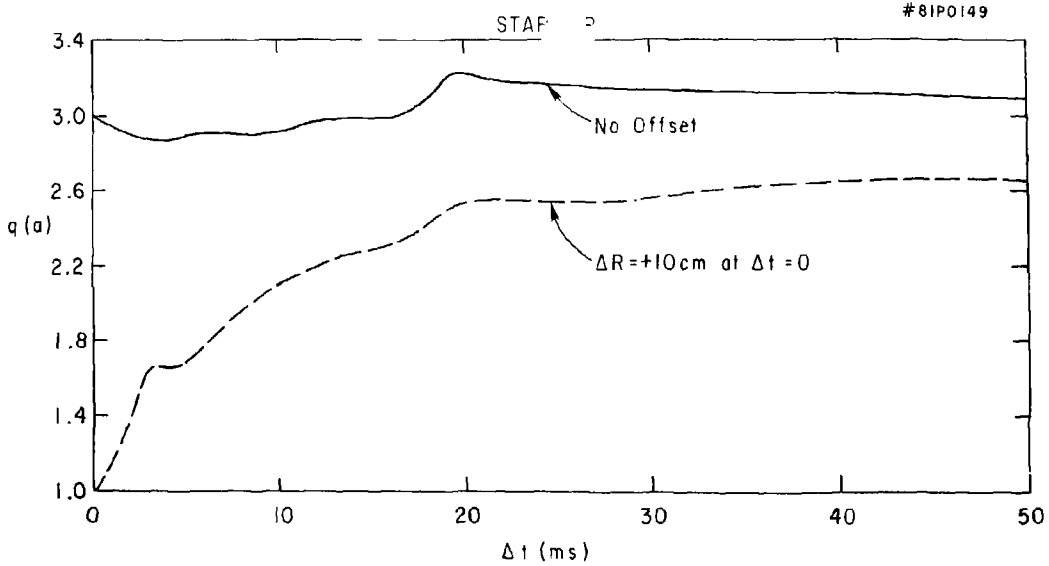
#81P0149
3.4
3.0
2.6
2.2
1.8
1.4
1.0
q(a)
No Offset
ΔR=+10cm at Δt=0
0
10
20
30
40
50
Δt (ms)

Fig. 17

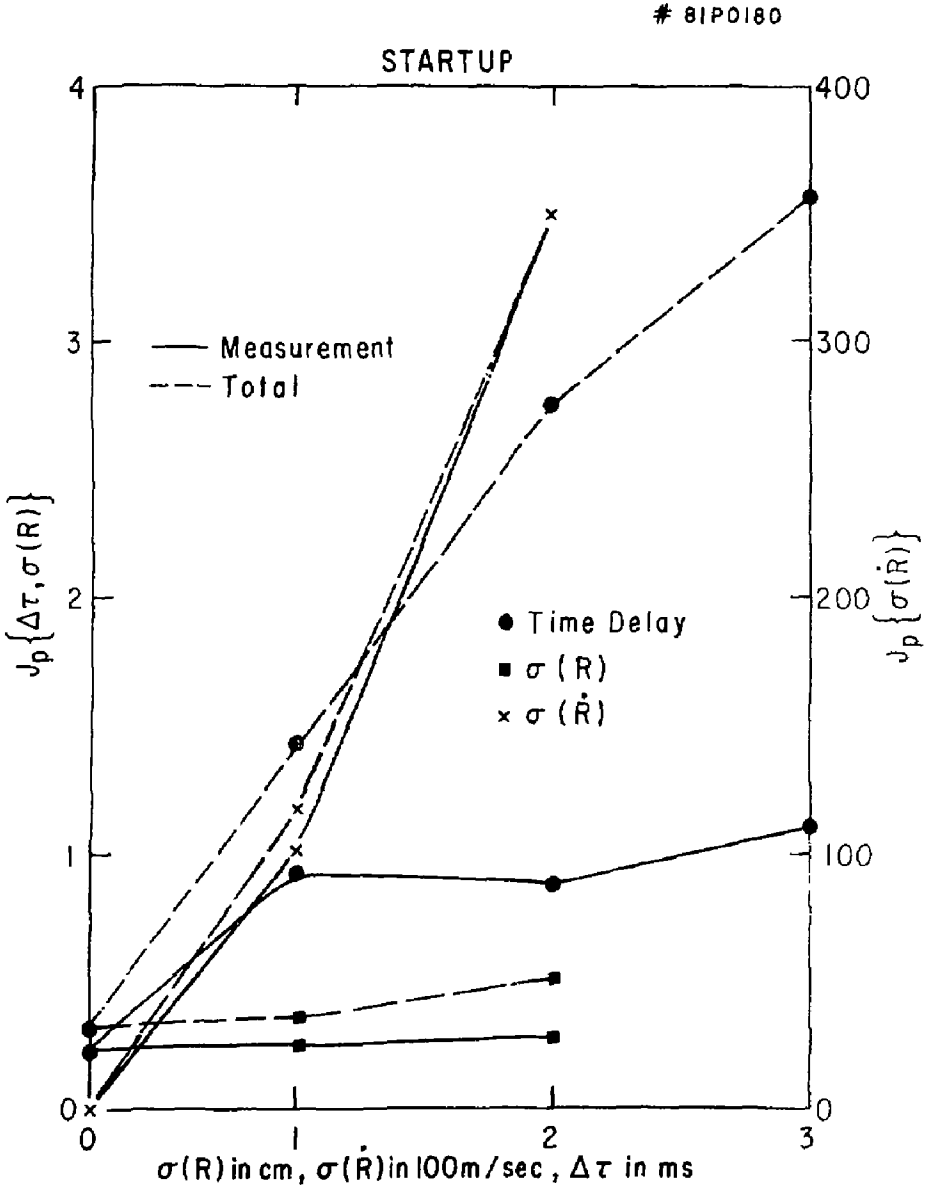
81P0180
STARTUP
Measurement
Total
Time Delay
σ (R)
σ (Ṙ)
$J_p\{\Delta\tau, \sigma(R)\}$
$J_p\{\sigma(\dot{R})\}$
σ(R) in cm, σ(Ṙ) in 100m/sec, Δτ in ms

Fig. 18

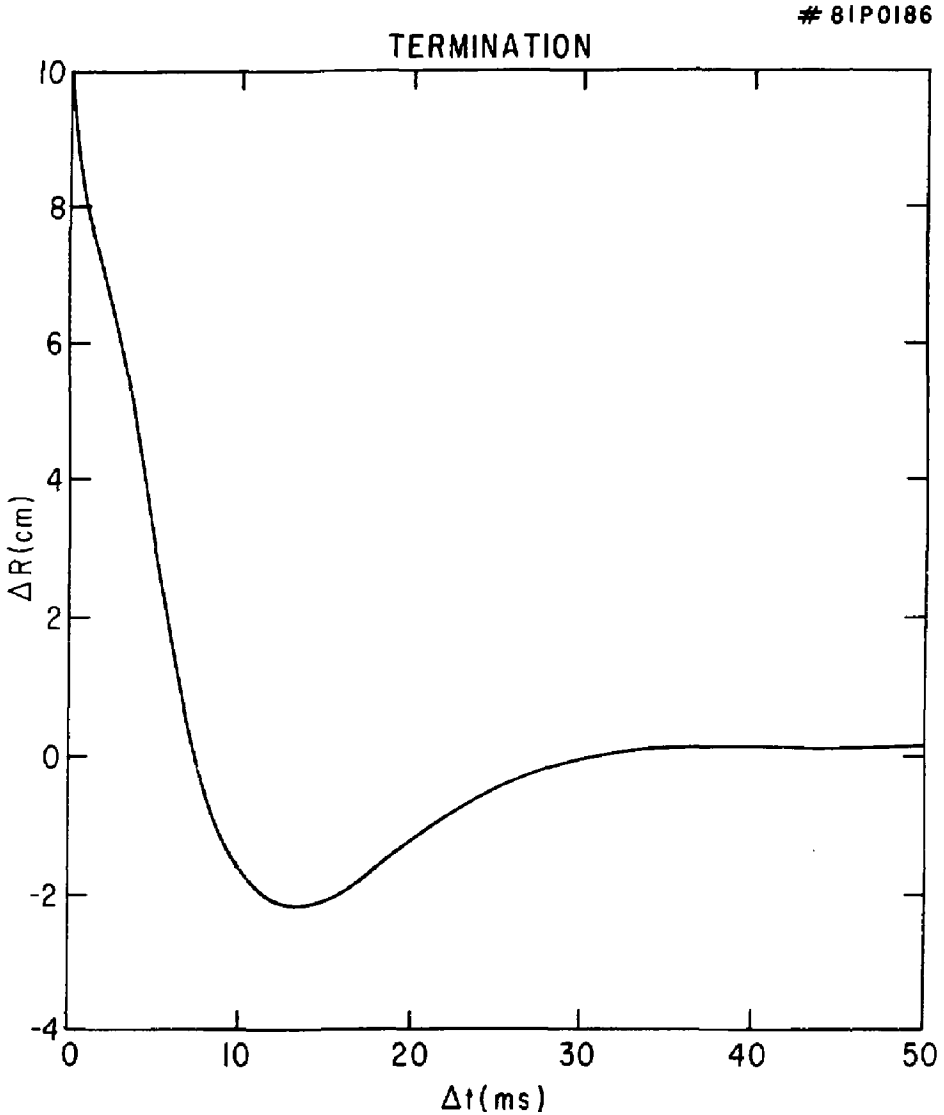

Fig. 19

81P0183

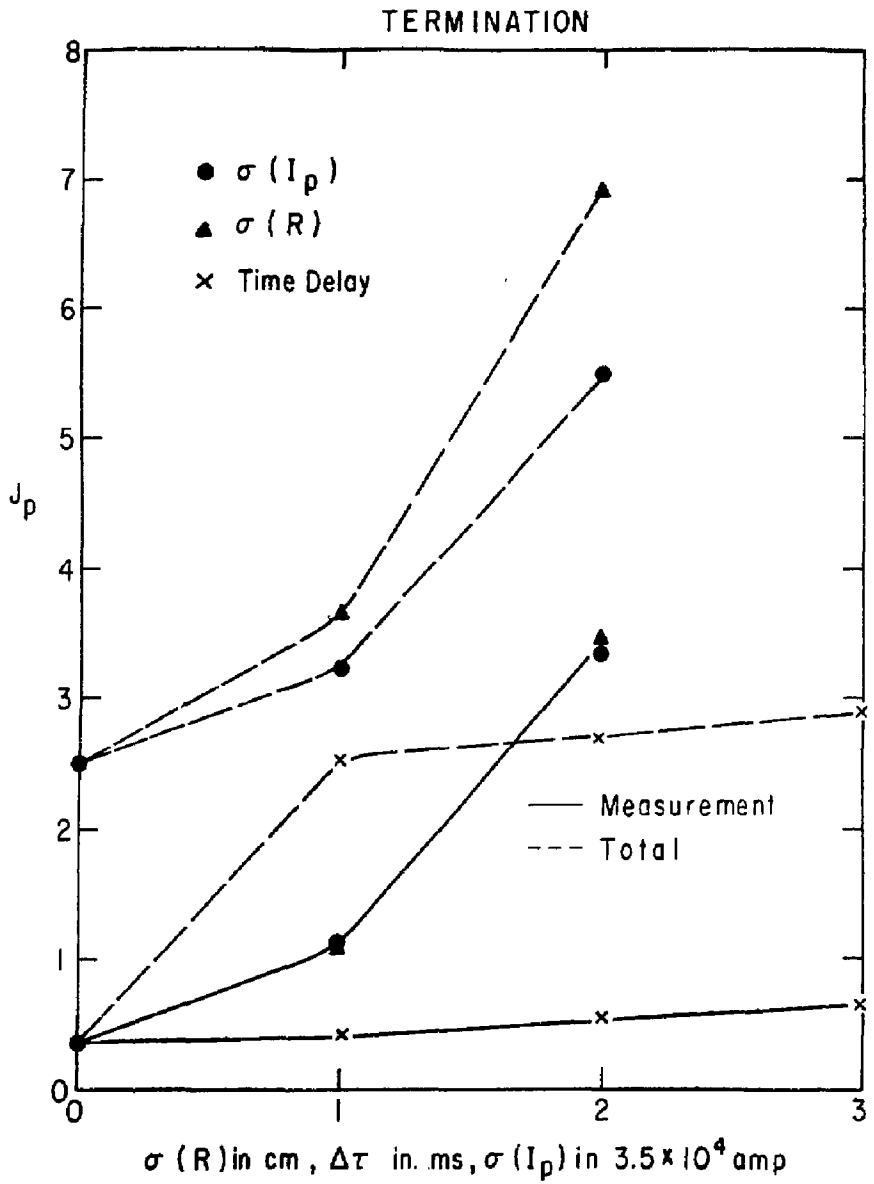

Fig. 20